

Article

Spatiotemporal Dynamics and Drivers of Wind Erosion during 1990–2020 in the Yarlung Zangbo River Basin, Southern Tibetan Plateau

Xiaomin Qin ^{1,2}, Dongmei Zhao ^{1,2}, Baojun Zhang ¹, Donghong Xiong ^{1,3,*}, Zhengrong Yuan ^{1,2}, Wenduo Zhang ^{1,2}, Lin Liu ^{1,2}, Dil Kumar Rai ^{1,2}, Sheikh Laraib ^{1,2} and Wei Deng ^{1,4}

¹ Key Laboratory of Mountain Hazards and Earth Surface Process, Institute of Mountain Hazards and Environment, Chinese Academy of Sciences, Chengdu 610299, China; qinxiaomin20@mails.ucas.ac.cn (X.Q.); zhaodongmei@imde.ac.cn (D.Z.); bjzhang@imde.ac.cn (B.Z.); yzhr@imde.ac.cn (Z.Y.); zhangwenduo@imde.ac.cn (W.Z.); lliu@imde.ac.cn (L.L.); dilkumarrai.geog@mails.ucas.ac.cn (D.K.R.); sheikhlaraib@imde.ac.cn (S.L.); dengwei@sicnu.edu.cn (W.D.)

² University of Chinese Academy of Sciences, Beijing 100049, China

³ Kathmandu Center for Research and Education, Chinese Academy of Sciences-Tribhuvan University, Beijing 100101, China

⁴ College of Geography and Resources Science, Sichuan Normal University, Chengdu 610101, China

* Correspondence: dhxiong@imde.ac.cn

Abstract: Wind erosion is recognized as one of the main environmental issues and seriously threatens ecosystem services in the Yarlung Zangbo River basin (YZRB), southern Tibetan Plateau. Exploring the spatiotemporal dynamics and drivers of wind erosion is crucial for improving regional ecosystem services and sustainable development. This study was conducted to examine the spatiotemporal patterns of soil wind erosion modulus (SWEM) in YZRB from 1990 to 2020 by using the revised wind erosion equation (RWEQ) and to identify the influence of climate change and anthropogenic activities on wind erosion dynamics. The results showed that temporally, the overall SWEM presented a significant downward trend ($-0.912 \text{ t} \cdot \text{hm}^{-2} \cdot \text{a}^{-1}$) and a continuous downward trend in the key implementation areas of ecological engineering. Spatially, the severe area of wind erosion is mainly concentrated in the flat and broad river valley, where sand sources are widely distributed. Significant SWEM differences were found among various land use/cover (LULC) types. Exceeding 90% reduction rates in SWEM occurred in forests, grasslands, and cultivated land. Additionally, the influence analysis showed that climate change was the dominant factor driving the variations in wind erosion due to the reduction of wind speed. By contrast, the contribution of anthropogenic activities is relatively less, accounting for 43.50% of wind erosion change, which closely matches the transfer of LULC to grassland and forest land with the implementation area of ecological engineering projects. This study provides useful information on the driving mechanism of wind erosion, prevention service changes, and determining priority zones for desertification prevention in YZRB. We suggest that eco-restoration activities should be endorsed in the future, as well as the adaptive management that is required to control wind erosion and improve ecosystem services and human well-being for people in the YZRB region.

Keywords: wind erosion; climate change; anthropogenic activity; revised wind erosion equation; Yarlung Zangbo River basin; Tibetan Plateau



Citation: Qin, X.; Zhao, D.; Zhang, B.; Xiong, D.; Yuan, Z.; Zhang, W.; Liu, L.; Rai, D.K.; Laraib, S.; Deng, W. Spatiotemporal Dynamics and Drivers of Wind Erosion during 1990–2020 in the Yarlung Zangbo River Basin, Southern Tibetan Plateau. *Land* **2023**, *12*, 1685. <https://doi.org/10.3390/land12091685>

Academic Editor: Vincent Chaplot

Received: 22 July 2023

Revised: 23 August 2023

Accepted: 24 August 2023

Published: 28 August 2023



Copyright: © 2023 by the authors. Licensee MDPI, Basel, Switzerland. This article is an open access article distributed under the terms and conditions of the Creative Commons Attribution (CC BY) license (<https://creativecommons.org/licenses/by/4.0/>).

1. Introduction

Soil erosion is the most widespread form of soil degradation [1]. Soil wind erosion manifests itself in the erosion, transport, and deposition of soil particles by wind. Macroscopically, it shows a series of major environmental changes, such as soil layer erosion, soil coarsening, and soil desertification, and affects ecological risks. Around one-third of the global land is affected by soil wind erosion, of which more than 50% is severely eroded [1–3].

Soil wind erosion has many adverse effects on the health of terrestrial ecosystems and the development of human society [4], such as significantly reducing soil fertility and plant productivity [5], resulting in reduced air quality [6]. In addition, fine-grained materials formed by surface wind erosion are the main source of atmospheric aerosols, providing a source of dust storms [7]. Therefore, it is crucial to evaluate the regional wind erosion intensity and analyse its influencing factors to provide a base for wind erosion prediction and desertification control.

The occurrence of soil wind erosion is a rather complex process that is the result of the combined effects of multiple factors, including topography, climate, and surface soil characteristics [8]. Climate change may have an impact on soil health and productivity as a result of accelerated or decelerated rates of erosion [9]. Wind speed, temperature, and precipitation are the main climatic factors that trigger soil wind erosion [10]. Among them, wind is considered the primary climatic factor that affects soil erosion. Additionally, the transportation of soil particles in arid and semi-arid regions through near-surface wind has a significant impact on the process of wind erosion [10]. As wind speed exceeds a certain threshold, the proportion of coarse particles in the eroded sediment increases [11]. As changes in precipitation occurrences occur, soil moisture content could result in differences in the soil texture and other soil properties [12]. Precipitation changes on a scale of more than 10 years can drive changes in vegetation function types, while annual and seasonal changes in precipitation can shift the phenology of vegetation and the coverage of ecosystems [13]. The importance of vegetation in safeguarding soils from wind erosion has been acknowledged for a considerable time. This is achieved by increasing the roughness of the surface and absorbing the downward momentum of the surrounding air current [14,15]. A strong correlation was suggested between vegetation cover and the total amount of soil loss, as previous studies [16,17] quantified a decrease in soil loss quantity that followed an exponential trend with increasing vegetation cover. The vegetation changes are usually represented by land use/cover change (LULC) [18]. The interaction between climate change and LULC also affects wind erosion [19]. LULC typically affects wind erosion by changing the natural landscape pattern [5]. Previously undertaken research findings have shown that LULC has a positive effect on reducing soil erosion in ecological projects [20,21]. Aside from the above driving factors, anthropogenic activities such as population, livestock, vegetation, and arable land were critical factors affecting aeolian desertification dynamics [22]. The lower plant coverage caused by grazing results in more soil being exposed to the air, leading to increased soil temperatures and soil wind erosion [23]. Therefore, the analysis of individual and coupling effects between driving factors plays an important role in finding out the evolution of wind erosion.

The Tibetan Plateau (TP) is seriously affected by desertification, which has been a crucial environmental issue in recent years. Insufficient precipitation and frequent strong winds make the land prone to soil wind erosion in TP [24,25]. The Yarlung Zangbo River basin (YZRB), as the economic, political, and cultural center of Tibet [26], plays an important role in the economic development of TP. Due to the rich sand, dry and windy climate, and sparse and low vegetation, the aeolian geomorphology is extremely developed [27]. It has been facing the disturbances of desertification and wind erosion for a long time. In 2019, the total area of sandy land was 734.1 km², accounting for 3.7% of YZRB [28]. The widely distributed sandy land has become the main material source of wind erosion, affecting agricultural, social, and economic activities in the region.

TP serves as a crucial ecological barrier area, exhibiting a high level of vulnerability and sensitivity to global climate change in terms of its ecosystem [29]. In the past few decades, there has been a pronounced warming trend observed in TP compared to other regions worldwide [30,31]. Additionally, there has been a slight increase in precipitation with noticeable spatial variations [32]. Continuously changing climatic conditions will have a certain impact on soil and wind erosion in the TP. To overcome desertification and wind erosion, the government has implemented a large number of ecological projects in YZRB since the 1990s, such as the Environmental Protection Programs [33]. Most of

these ecological projects involve the implementation of afforestation activities and graze closures, which directly contribute to the changes in LULC. As a result, there has been a significant improvement in the ecological landscape and a substantial reduction in the extent of wind-sandy land [34]. However, little attention has been devoted to the impact of these projects on wind erosion and the driving factors. In the context of significant changes in climate and anthropogenic activities, it is of great significance to study the temporal and spatial dynamics of wind erosion in YZRB, which can provide a theoretical basis for the implementation and layout decisions of subsequent ecological projects.

Despite significant efforts and contributions to TP made by previously undertaken research, scientific research on soil wind erosion in the YZRB region has insufficient data, due to slow data updating and a lack of long-term or new data. Currently, few studies have been undertaken to explore the driving factors behind wind erosion in YZRB. Meanwhile, understanding the impact of ecological engineering on regional soil and wind erosion changes is unknown and inadequate so far. Hence, the specific objectives of this study are: (1) to investigate the spatiotemporal dynamics of the wind erosion in YZRB from 1990 to 2020 by using the revised wind erosion equation (RWEQ); (2) to assess the correlations between wind erosion dynamics among climatic factors such as wind speed, precipitation, and forest vegetation cover (FVC); and (3) to quantify the relative contribution rates of climate change and human activities to wind erosion dynamics. The findings of this study could provide insights into the driving factors of wind-driven erosion dynamics and the fundamental guidelines for ecological management and sustainable development in the YZRB.

2. Materials and Methods

2.1. Study Area

The middle section of the YZRB valley is located in the south of the Tibetan Plateau (Figure 1a), spanning across 12 counties (cities) that cover an area of 20,123.2 km². It is geographically situated between 28°55′ N and 30°19′ N and 92°22′ E and 92°37′ E. This region has a plateau temperate monsoon semi-arid climate, characterized by dry and windy conditions during winter and spring with a long duration. The average annual precipitation ranges from 300 to 450 mm, with the majority occurring between June and September, accounting for over 90% of the annual precipitation [35]. Evaporation measures 2688.5 mm. The presence of vast expanses of sandy terrain in this area persists as a significant environmental challenge brought about by the deleterious effects of human activities and climate change [28]. The region also encompasses 523.1 km² of desertified area [36], which exhibits a patchy and discontinuous distribution along both sides of the river valley. The predominant soil types in this area consist of aeolian sand soil and newly accumulated soil, characterized by a short period of soil formation, rapid water infiltration, high evaporation rates, and limited water and nutrient retention capabilities. The primary vegetation comprises mountain thickets, grasslands, and alpine meadows [28].

2.2. Data Sources

The meteorological data from weather stations in the central region of YZRB were obtained from the China Meteorological Science Data Service Centre (<http://www.nmic.cn/> (accessed on 5 September 2021)) for the period of 1990 to 2020 (Table 1). The data includes daily measurements of wind speed, precipitation, air temperature, and sunshine duration. Additionally, we processed and interpolated the data, generating 1 km × 1 km grid data to supplement our analysis. The snow depth time series dataset was obtained through the National Cryosphere Desert Data Centre (<http://www.ncdc.ac.cn/portal/> (accessed on 7 September 2021)). Furthermore, we incorporated a soil data set including soil properties on the scale of (1:10,000,000) specific to cold and arid regions, obtained from the Harmonized World Soil Database (<https://www.fao.org/> (accessed on 7 September 2021)). The processed dataset encompasses various soil types and their corresponding physical and chemical properties, spanning 1 km × 1 km. For the Digital Elevation Model (DEM),

we utilized the NASA product SRTM (Shuttle Radar Topography Mission) DEM with 30 m of spatial resolution. The normalized difference vegetation index (NDVI) data was utilized to assess the vegetation in YZRB. The annual NDVI time series data spanning the years 1990–2020 that is available at $1 \text{ km} \times 1 \text{ km}$ spatial resolution was acquired from the National Tibetan Plateau Data Centre (<http://data.tpd.cn/zh-hans/> (accessed on 10 September 2021)). The livestock datasets used in our analysis were also acquired from the same source (<http://data.tpd.cn> (accessed on 15 September 2021)). In addition, all data achieve the same resolution by resampling and other methods.

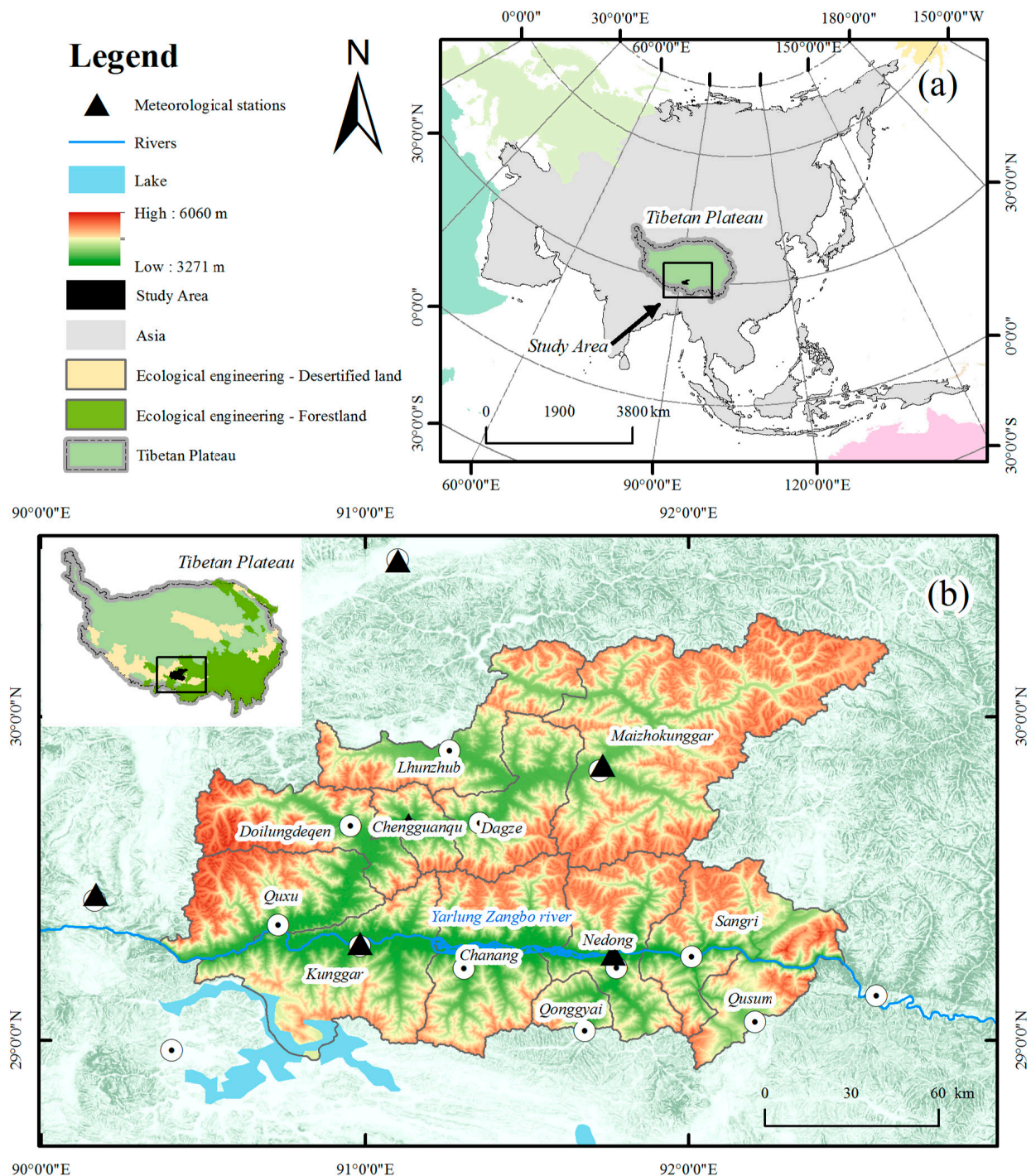


Figure 1. (a) The study area is located in Asia. (b) Map showing the spatial pattern of elevation in the Yarlung Zangbo River basin (YZRB).

Table 1. Summary of forcing data used in the Revised Wind Erosion Equation (RWEQ).

Data	Description	Resolution	Time
Climate data	Wind speed	1 km × 1 km	1990–2020
	Temperature		
	Precipitation		
	Solar radiation		
Vegetation data	NDVI	1 km × 1 km	1990–2020
livestock data	Actual livestock carrying capacity estimation product	1 km × 1 km	2000–2020
Land-use data	China multi-period land use remote sensing monitoring data set (CNLUCC)	1 km × 1 km	1990–2020
Soil data	Harmonized World Soil Database v 1.2 (HWSD)	1:10,000,000	2020
Elevation data	SRTM (Shuttle Radar Topography Mission)	30 m × 30 m	2020
Snow depth	Long-term series of daily snow depth dataset in China	25 km × 25 km	1990–2020

2.3. Methods

2.3.1. Soil Wind Erosion Modulus

In this study, the RWEQ was used to calculate wind-induced soil erosion and sand fixation [37], which has the advantages of relatively comprehensive factors, relatively simple composition, easy data acquisition, and a strong affinity with the geographic information system. It can combine field data with computer models to describe physical wind erosion processes [38] and has been widely used in practice. In addition, the calculated results of this model have a high degree of fitting with the measured values. The calculation formula is as follows:

$$Q_{max} = 109.8 \times WF \times EF \times K' \times SCF \times C \quad (1)$$

$$S = 150.71 \times (WF \times EF \times K' \times SCF \times C)^{-0.3711} \quad (2)$$

$$S_L = \frac{2z}{S^2} Q_{max} \times e^{-\left(\frac{z}{S}\right)^2} \quad (3)$$

where, S_L is the actual wind erosion modulus (kg/m^2); Q_{max} is the maximum transport capacity (kg/m); S is the critical field length (m); z is the distance from the upwind edge of the field. WF is the weather factor (kg/m); EF and SCF are soil erodibility factors and soil crust factors, respectively; K' and C are soil roughness factors and vegetation factors, respectively.

The main factor calculation method of the RWEQ model is as follows:

(1) Climatic factor

The climatic factors in the RWEQ model represent the comprehensive effect of weather factors such as wind speed, temperature, precipitation, and snow depth on soil wind erosion in the study area, which is one of the core factors of the model. The calculation method is as follows:

$$WF = W_f \times SW \times SD \times \frac{\rho}{g} \quad (4)$$

$$W_f = u_2 \times (u_2 - u_1)^2 \times N_d \quad (5)$$

WF is weather factor (kg/m); W_f is wind factor (m/s^3); g is gravity acceleration ($9.8 \text{ m}/\text{s}^2$); ρ is air density; SW and SD are soil moisture factors and snow cover factors, respectively; u_1 is the sediment wind speed; u_2 is the monthly mean wind speed (m/s); and N_d is the number of days with a monthly wind speed greater than the sediment wind speed.

SW is a soil moisture factor, and its size is negatively correlated with wind erosion rate. The calculation formula for the soil moisture factor is as follows:

$$SW = \frac{ET_p - (R + I) \times \frac{R_d}{N_d}}{ET_p} \quad (6)$$

$$ET_p = 0.0162 \times \frac{SR}{58.5} (DT + 17.8) \quad (7)$$

SW represents soil moisture factor; ET_p represents potential evaporation (mm); R_d represents the days of precipitation or irrigation during the measurement period (d); $R + I$ represents rainfall and irrigation amount (mm); and N_d is the number of days with a monthly wind speed greater than sediment wind speed.

SD represents the snow cover factor, and a certain degree of snow can weaken the soil through wind erosion. In general, when the snow thickness is greater than 25.4 mm, soil wind erosion tends to stop. The calculation formula for the snow cover factor is as follows:

$$SD = 1 - P(H_{snow} > 25.4\text{mm}) \quad (8)$$

where H_{snow} represents snow thickness (mm) and P represents the probability of snow cover depth greater than 25.4 mm.

(2) Soil erodibility factor

Soil particle size and organic matter, calcium carbonate, and clay content will affect the size of soil erodibility. The calculation method is:

$$EF = \frac{29.9 + 0.31sa + 0.71si + 0.33\left(\frac{sa}{cl}\right) - 2.59OM - 0.95CaCO_3}{100} \quad (9)$$

EF is a soil erodibility factor; sa is soil coarse sand content (%); cl is soil clay content (%); OM is organic matter content (%); $CaCO_3$ is calcium carbonate content (%);

(3) Soil crust factor

Hard soil crusts can effectively prevent the occurrence of soil wind erosion. Therefore, the soil crust factor is usually used to characterize the effective wind erosion resistance of hard soil crust on the soil surface. The formula is as follows:

$$SCF = \frac{1}{1 + 0.0066(CL)^2 + 0.021(OM)^2} \quad (10)$$

(4) Vegetation factor

The vegetation factor indicates the degree of inhibition of soil wind erosion under certain vegetation coverage; the formula is as follows:

$$C = e^{-0.0438SC} \quad (11)$$

SC is vegetation coverage (%).

(5) Surface roughness factor

The Surface roughness factor is the influence of surface roughness caused by topography on soil wind erosion. The calculation formula is as follows:

$$K' = e^{(1.86K_r - 2.41K_r^{0.934} - 0.127C_{rr})} \quad (12)$$

$$K_r = 0.2 \frac{(\Delta H)^2}{L} \quad (13)$$

where C_{rr} is the random roughness factor (cm); K_r is the terrain roughness factor (cm); L is the terrain fluctuation parameter; ΔH is the elevation difference (m) within the range of L .

2.3.2. Spatiotemporal Trend Analysis

The Mann-Kendall (MK) trend test [39,40] and Sen's slope estimator methods [41] were employed to assess the significance and direction of the wind erosion change trend. The MK trend test method offers flexibility, robustness, and widespread applicability, making it a valuable tool for trend analysis in many different research areas. The Hurst Exponent is usually used to describe the consistency of time series changes [42]. The Hurst exponent provides valuable insights into the behavior of time series data, particularly in terms of long-term memory and scaling properties. Its ability to detect long-range dependence and its applicability to a wide range of fields make it a useful tool for analyzing complex systems and identifying underlying patterns in data. By combining these three methods, it becomes possible to not only elucidate the current trends in time series but also provide some degree of future trend prediction (Table 2). The calculation formula is as follows:

Table 2. Mann-Kendall test trend categories.

Q_i	Z	Trend Type	Trend Features
$Q_i > 0$	$2.58 < Z$	4	Very significant increase
	$1.96 < Z < 2.58$	3	Significantly increase
	$1.65 < Z < 1.96$	2	Micro-significant increase
$Q_i = 0$	$Z \leq 2.58$	1	No significant increase
	Z	0	No Change
	$Z \leq 1.65$	−1	No significant decrease
$Q_i < 0$	$1.65 < Z < 1.96$	−2	Micro-significant decrease
	$1.96 < Z < 2.58$	−3	Significantly decrease
	$2.58 < Z$	−4	Very significant decrease

The MK trend test is based on two hypotheses: one is null (H_0), and the other is the alternative (H_1). H_0 expresses the existence of no trend, while H_1 elucidates a significant rising or declining trend in the data. On the basis of a 5% significance level, if the p -value < 0.05 , then the alternative hypothesis is accepted, which signifies the presence of a trend in the data, and if the p -value > 0.05 , the H_0 will be accepted, which denotes the absence of a trend in the data. The formula is provided by the following equation:

$$S = \sum_{i=1}^{n-1} \sum_{j=i+1}^n \text{sign}(X_j - X_i) \quad (14)$$

where n is the number of data points, X_j and X_i are annual values in years j and i , $j > i$, and $\text{Sign}(X_j - X_i)$ calculated using the equation:

$$\text{sign}(X_j - X_i) = \begin{cases} -1 & \text{for } (X_j - X_i) < 0 \\ 0 & \text{for } (X_j - X_i) = 0 \\ +1 & \text{for } (X_j - X_i) > 0 \end{cases} \quad (15)$$

The test of Sen's slope estimator was originally developed by Sen for the purpose of checking statistical linear relationships. It is used to calculate the magnitude of trends in long-term temporal data. Sen's slope is considered better to detect the linear relationship as it is not affected by outliers in the data. The following equation is used to estimate each individual slope (Q_i):

$$Q_i = \frac{Y_j - Y_i}{j - i} \quad (16)$$

where $i = 1$ to $n - 1$, $j = 2$ to n , and Y_j and Y_i are data values at time j and i ($j > i$), respectively. If, in the time series, there are n values of Y_j , estimates of the slope will be $N = n(n - 2)/2$. The slope of the Sen estimator is the mean slope of such slopes' N values. The Sen's slope is:

$$Q_i = \begin{cases} \frac{Y_j - Y_i}{j - i} & \text{if } n \text{ is odd} \\ \frac{1}{2} \left(Q_{\frac{N}{2}} + Q_{\left[\frac{N+2}{2} \right]} \right) & \text{if } n \text{ is even} \end{cases} \quad (17)$$

The positive (Q_i) indicates an increasing trend, while the negative Q_i values tell us that there is a negative trend in the temporal data. The unit of Sen's slope (Q_i) is the slope magnitude per year.

$$Var(S) = \frac{n(n + 1)(2n + 5)}{18} \quad (18)$$

When $n > 10$, the standard normal statistical variable Z is:

$$Z = \begin{cases} \frac{S}{\sqrt{Var(S)}} & (S > 0) \\ 0 & (S = 0) \\ \frac{S+1}{\sqrt{Var(S)}} & (S < 0) \end{cases} \quad (19)$$

2.3.3. Partial Correlation Analysis

The partial correlation analysis was conducted to explore the relationship between wind erosion and individual climatic deriving factors while controlling for the influence of other climate factors. The calculation formula is as follows:

$$r_{ya,bc}^2 = \frac{r_{ya,b} - r_{yc,b}r_{ac,b}}{\sqrt{(1 - r_{yc,b}^2)(1 - r_{ac,b}^2)}} \quad (20)$$

$$t = \frac{r_{ya,bc}}{\sqrt{(1 - r_{ya,bc}^2)}} \sqrt{n - m - 1} \quad (21)$$

where, $r_{ya,bc}$ is the partial correlation coefficients between y and a , excluding the influence of b and c ; $r_{ya,b}$ is the partial correlation coefficients between y and a , excluding the influence of b ; $r_{yc,b}$ is the partial correlation coefficients between y and c , excluding the influence of b ; $r_{ac,b}$ is the partial correlation coefficients between c and a , excluding the influence of b ; where n is the sample size and m is the number of independent variables.

2.3.4. Multiple Correlation Analysis

Multiple correlation analysis is used to quantify the degree of correlation between a single variable and multiple variables. The composite impact of maximum wind speed, precipitation, and FVC on wind erosion is expressed using multiple correlation coefficients. The calculation formula is shown as follows:

$$R_{y,abc}^2 = \sqrt{1 - (1 - r_{ya}^2)(1 - r_{yb,a}^2)(1 - r_{yc,ab}^2)} \quad (22)$$

2.3.5. Calculation of Driving Factor

Due to the interaction among natural factors, we considered nine dominant driving factors (Table 3). Partial correlation coefficients were used to measure the correlation between two variables after eliminating the influence of other variables. Multiple correlation coefficients were used to characterize the interactive effects of different natural factors on wind erosion. Then, the dominant factors were determined using the following criteria based on the partial correlation coefficients and complex correlation coefficients.

Table 3. The basis of driving factors.

Dominant Driver	Basis			
	$R_{sl-FVC,P \& W}$	$R_{sl-P,W \& FVC}$	$R_{sl-W,P \& FVC}$	$R_{sl-W \& P \& FVC}$
Strong drive (W + P + FVC)	$ t > t_{0.05}$	$ t > t_{0.05}$	$ t > t_{0.05}$	$F > F_{0.05}$
Strong drive (P + FVC)	$ t > t_{0.05}$	$ t > t_{0.05}$	$ t \leq t_{0.05}$	$F > F_{0.05}$
Strong drive (W + FVC)	$ t > t_{0.05}$	$ t \leq t_{0.05}$	$ t > t_{0.05}$	$F > F_{0.05}$
Strong drive (W + P)	$ t \leq t_{0.05}$	$ t > t_{0.05}$	$ t > t_{0.05}$	$F > F_{0.05}$
Strong drive (FVC)	$ t > t_{0.05}$	$ t \leq t_{0.05}$	$ t \leq t_{0.05}$	$F > F_{0.05}$
Strong drive (P)	$ t \leq t_{0.05}$	$ t > t_{0.05}$	$ t \leq t_{0.05}$	$F > F_{0.05}$
Strong drive (W)	$ t \leq t_{0.05}$	$ t \leq t_{0.05}$	$ t > t_{0.05}$	$F > F_{0.05}$
Weak drive (W + P + FVC)	$ t \leq t_{0.05}$	$ t \leq t_{0.05}$	$ t \leq t_{0.05}$	$F > F_{0.05}$
Non-climatic factor drive				$F \leq F_{0.05}$

Where W represents maximum wind speed; P represents precipitation, and FVC represents vegetation cover. $R_{sl-FVC,W \& P}$ is the Student's t -test for the partial correlation of wind erosion with vegetation cover and maximum wind speed, $R_{sl-FVC,P \& W}$ is the Student's t -test for the partial correlation of wind erosion with FVC and precipitation, $R_{sl-P,W \& FVC}$ is the Student's t -test for the partial correlation of wind erosion with precipitation and maximum wind speed, and $R_{sl-W \& P \& FVC}$ is the F -test for the composite correlation coefficient of wind erosion with the three independent variables. $t_{0.05}$ is the critical value of the Student's t -test statistic at a 0.05 significance level, and $F_{0.05}$ is the critical value of the F -test statistic at a 0.05 significance level.

3. Results

3.1. Temporal and Spatial Variation in Soil Wind Erosion Modulus

The overall SWEM from 1990 to 2020 and the wind erosion area gradually shrank from the surrounding area of the basin to the middle valley area. The mean annual SWEM was $3.85 \text{ t} \cdot \text{hm}^{-2}$, with the highest SWEM ($27.46 \text{ t} \cdot \text{hm}^{-2}$) in 1994 and the lowest SWEM ($0.01 \text{ t} \cdot \text{hm}^{-2}$) in 2020. Relative to 1990, the annual SWEM decreased by nearly 93% in 2020 in the whole region, with a rate of $-0.912 \text{ t} \cdot \text{hm}^{-2} \cdot \text{a}^{-1}$. The spatial variation of average SWEM is evident, with the highest values primarily concentrated in the valleys (Figure 2b). In 1993, the SWEM recorded an exceptionally high value of $608.58 \text{ t} / \text{hm}^2$ in this area, which coincided with a relatively concentrated distribution of sandy land in the valleys. This is highly correlated with the previous research finding that the Shannan Wide Valley witnesses an annual sediment deposition exceeding 780,000 tons [43], leading to the exposure of numerous central shoals and floodplains during the dry season. Results of the applied MK and Sen's slope estimator statistical tests for soil wind erosion are presented in Figure 2a. The overall wind erosion within the YZRB underwent notable changes, predominantly characterized by a significant reduction from 1990 to 2020. Specifically, a total area of $18,863 \text{ km}^2$ displayed a downward trend, constituting approximately 93.76% of the region, whereas an area of 316 km^2 exhibited an upward trend, accounting for approximately 1.57%. Furthermore, 5.87%, 22.41%, and 55.71% of the area experienced no significant decrease, a minor yet statistically significant decrease, and a significant decrease ($p < 0.05$) in wind erosion, respectively. The areas with a significant decrease were primarily concentrated in the flood plain and southern banks of Kunggar and Chanang counties. This phenomenon can be attributed to the initial focus of planting activities near densely populated areas, such as towns along the southern bank, gradually expanding towards the river bank and central flood plain.

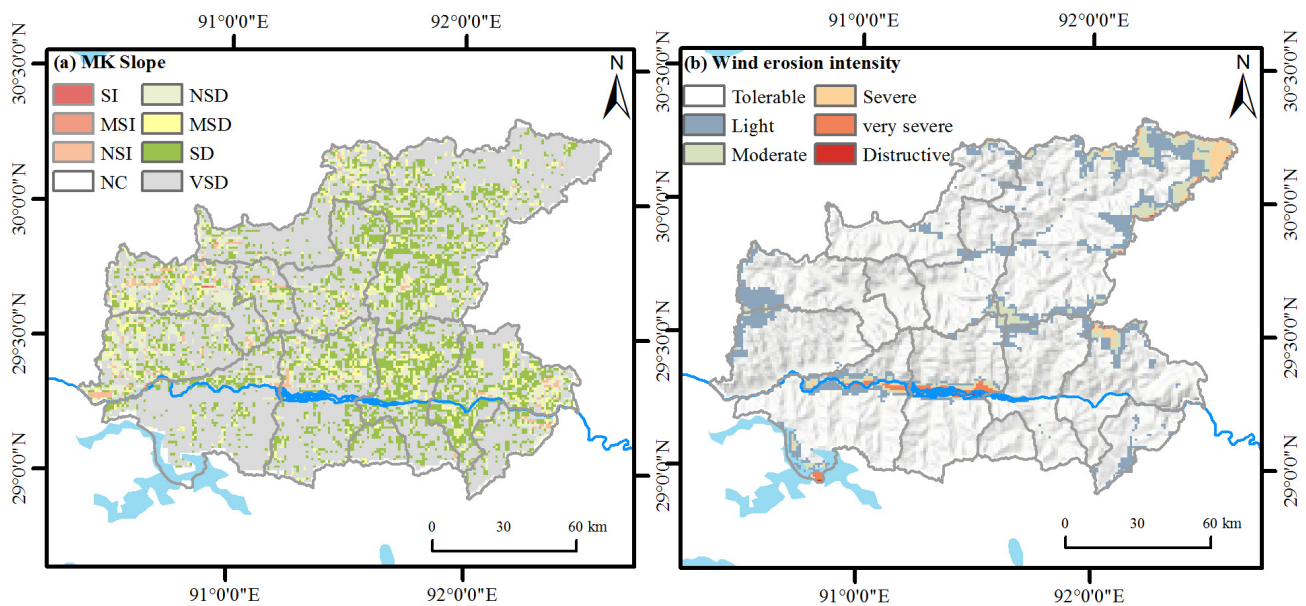


Figure 2. The spatial patterns of the slope of MK trend test method (a) and average soil wind erosion intensity (b) in the study area; SI represents Significantly increase, MSI represents Micro-significant increase; NSI represents No significant increase; NC represents No Change; NSD represents No significant decrease; MSD represents Micro-significant decrease; SD represents Significantly decrease; VSD represents Very significant decrease.

According to the criterion system from the classification criteria for Classification and Gradation of Soil Erosion of China (SL190–2007), the wind erosion intensity in YZRB was categorized into six grades: tolerable ($<2 \text{ t} \cdot \text{hm}^{-2} \cdot \text{a}^{-1}$), light ($2\text{--}25 \text{ t} \cdot \text{hm}^{-2} \cdot \text{a}^{-1}$) moderate ($25\text{--}50 \text{ t} \cdot \text{hm}^{-2} \cdot \text{a}^{-1}$), severe ($50\text{--}80 \text{ t} \cdot \text{hm}^{-2} \cdot \text{a}^{-1}$), very severe ($80\text{--}150 \text{ t} \cdot \text{hm}^{-2} \cdot \text{a}^{-1}$) and destructive (greater than $150 \text{ t} \cdot \text{hm}^{-2} \cdot \text{a}^{-1}$). The areas with tolerable conditions were widely distributed, accounting for 91.52% of the study area, and were mainly distributed in forest and dense grassland (Figure 3). The soil wind erosion decreased year by year, especially in the tolerable and above areas. Regions with moderate, severe, very severe, and destructive erosion were mainly situated in the river valley, accounting for 8% of the study area.

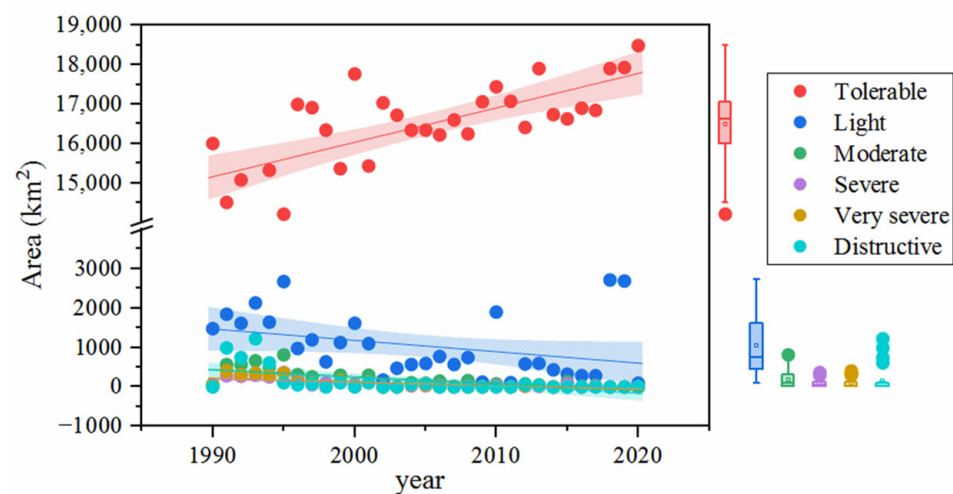


Figure 3. Schematic diagram of the wind erosion intensity in the study area.

3.2. Consistency of Future Wind Erosion Trend

The Hurst Exponent of wind erosion in YZRB from 1990 to 2020 is 0.46 (Figure 4a), indicating a weak and inconsistent trend of wind erosion. The area proportion of consistency is 34.12% and the area proportion of inconsistency is 65.88% in YZRB, which indicates the temporal and spatial change in wind erosion is fluctuating. According to the proportion of the area measured by ArcGIS, 7.93% of the areas show strong consistency in the future evolution trend, 45.47% of the areas show weak inconsistency, about 1.22% of the areas show strong inconsistency, and 22.15% of the areas show weak consistency (Figure 4b). In the future, the wind erosion trend in some areas may no longer be dominated by continuous reduction, with a total area of 13,284.68 km². However, the trend of wind erosion is still dominated by a continuous decline in areas with frequent human activities.

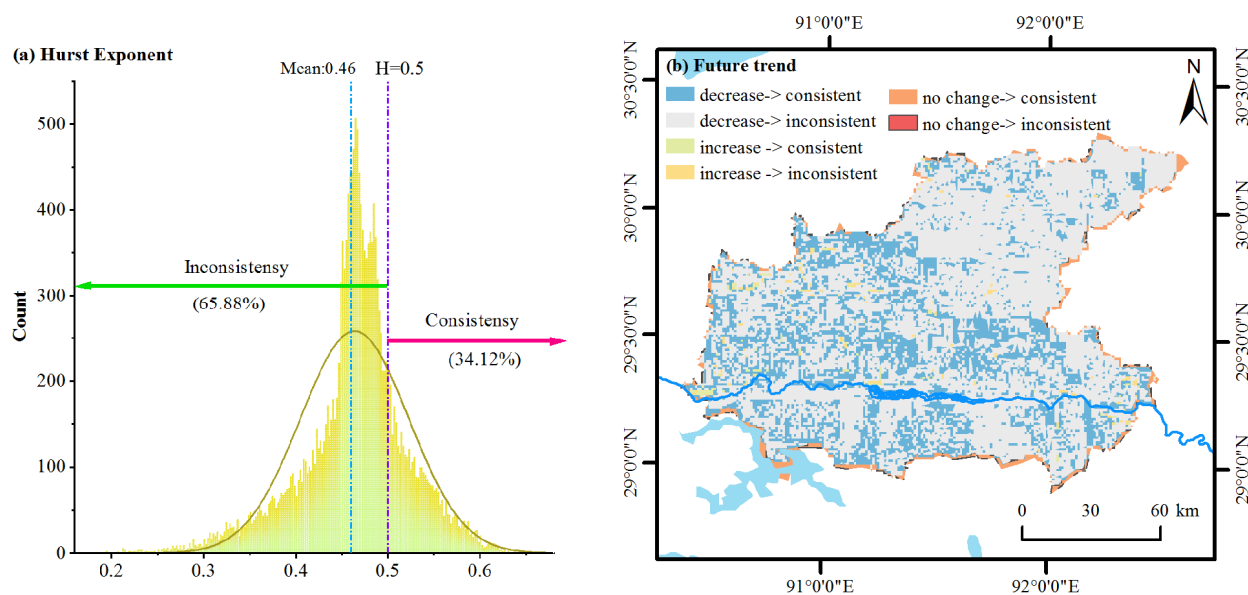


Figure 4. The histogram of Hurst Exponent (a) and the spatial patterns of future trend (b) of the study area from 1990 to 2020.

3.3. Driving Factor of Wind Erosion

We calculated the simple correlation coefficients between maximum wind speed, precipitation, FVC, and wind erosion. We found that maximum wind speed is positively correlated with wind erosion, with approximately 83% of the regions passing the significance test ($p < 0.05$). In contrast, only 6% of the regions have shown a negative correlation (Figure 5b). The correlation between precipitation and wind erosion showed a less strong correlation, with most regions representing a negative correlation, especially in the western part of the study area (Figure 5a). The FVC exhibits a similar pattern to the precipitation, primarily showing a negative correlation (Figure 5d), and most of these correlations occur in areas with better vegetation, which is consistent with the actual situation.

We generated a multiple correlation analysis graph among the three factors to differentiate their combined effects. The results indicate that when maximum wind speed is involved, the correlation coefficient is higher, suggesting that the combined effect of maximum wind speed and other factors has a certain impact on wind erosion. Under the influence of precipitation and maximum wind speed (Figure 5c), a noticeable inhibitory effect was observed near the water system, while a promoting effect was seen on the southern bank. In contrast, under the combined influence of maximum wind speed and FVC (Figure 5e), the multiple correlation coefficients exhibited significant differences, with higher values near the water system. However, when considering the effects of precipitation and FVC (Figure 5f), the main impact on wind erosion was inhibitory, with an average multiple correlation coefficient of 0.36, significantly lower than the value when all three factors were present (a 0.46 coefficient value).

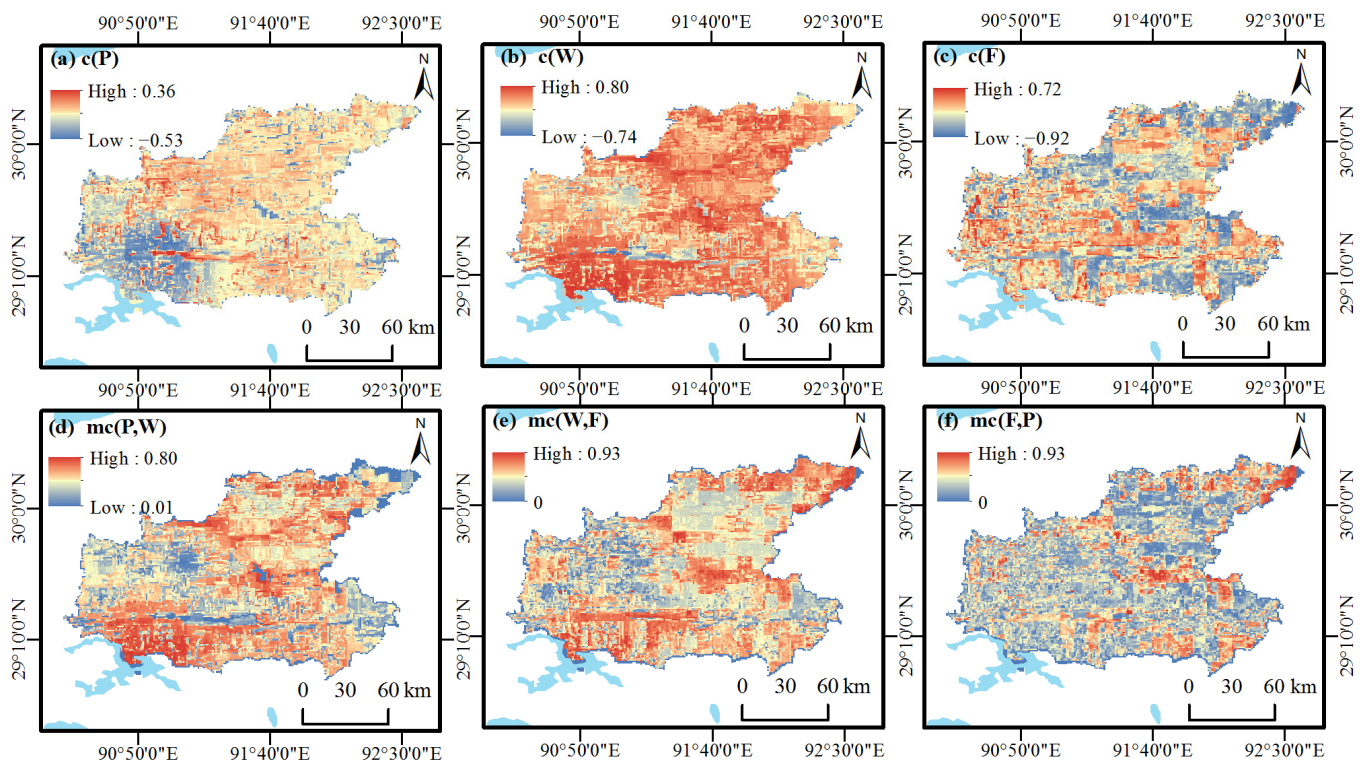


Figure 5. The spatial patterns of the simple correlation coefficient (a) between precipitation (P) and wind erosion, the simple correlation coefficient (b) between maximum wind speed (W) and wind erosion, the simple correlation coefficient (c) between FVC (F) and wind erosion, the spatial patterns of the multiple correlation coefficient (d) between precipitation (P) and maximum wind speed (W), the multiple correlation coefficient (e) between maximum wind speed (W) and FVC (F), and the multiple correlation coefficient (f) between FVC (F) and precipitation.

The occurrence and inhibition of wind erosion are intricate and connected to various factors. In this section, we present the distribution of driving forces for wind erosion in YZRB. Figure 6 illustrates that approximately 43.50% of the area is affected by anthropogenic activities. Conversely, areas with notable changes are primarily influenced by the alteration of maximum wind speed (28.62%) and FVC (10.36%). The impact of precipitation change in wind erosion is not significant, accounting for only 0.67%. Among the 55.71% of the area experiencing a significant decrease, the majority can be attributed to changes in maximum wind speed, indicating the crucial role of climate change. This signifies an opportune moment for implementing ecological engineering. The result revealed that the anomalous decrease pixels are mainly observed in forested areas and areas near construction sites, where ecological restoration programs and necessary urban environmental implementation activities have caused these changes.

3.4. Divergence of Soil Wind Erosion from Different Land Use/Land Cover Types

The changes in soil wind erosion modulus for different land use types were analyzed (Table 4), and the results indicate that unused lands such as sandy land and bare land have significantly higher soil wind erosion modulus compared to forest land. Specifically, the amount of wind erosion on sandy land in 1990 was 1803.66×10^3 t, much higher than that on shrub land (6.92×10^3 t). This finding can be attributed to the abundant sediment supply in floodplain areas, which serves as the primary source of wind erosion materials in the YZRB region. These areas have been characterized by less surface cover, an open terrain surface, and the presence of strong wind forces, resulting in severe soil wind erosion in these land types. This study further revealed that sandy land, forest, grassland, and cultivated land exhibited higher reduction rates in soil wind erosion modulus, with

reduction rates exceeding 90%. Particularly for sandy land, there was a significant decrease in wind erosion modulus during this study period, with a reduction rate of 92.87%. As key targets for windbreak and sand fixation, bare land and other unused lands showed a slightly lower reduction rate in soil wind erosion modulus, showing a reduction rate of 70.50% for bare land due to their specific geographical conditions, indicating a relatively weaker resistance to wind erosion compared to other land use/land cover types.

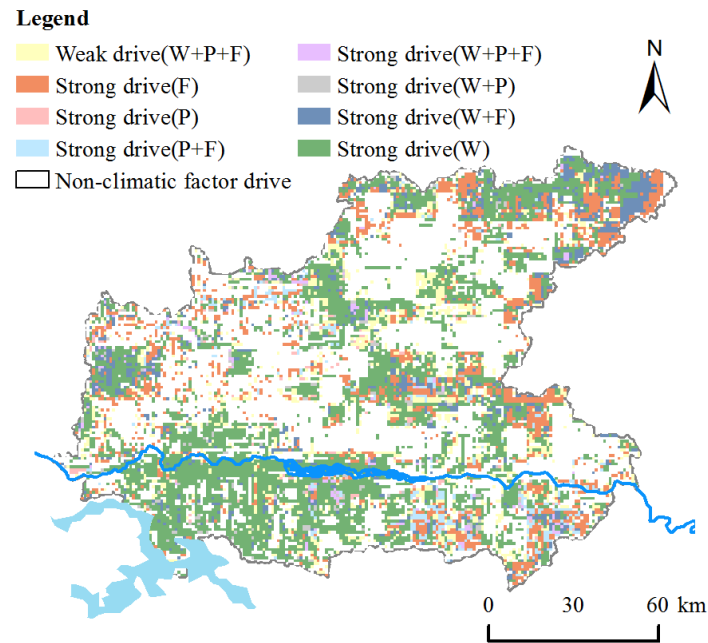


Figure 6. The spatial pattern of driving factors of climatic and anthropogenic factors on wind erosion dynamics in the study area from 1990 to 2020.

Table 4. The difference in the average soil wind erosion modulus (SWEM) of each land use/land cover type.

Land Use/Land Cover Type	S_L (10^3 t)			SWEM (t/hm^2)		
	1990	2020	Change Rate	1990	2020	Change Rate
Cultivated land	92.00	8.83	90.40%	1.02	0.08	−91.91%
Shrub land	6.92	5.42	21.68%	0.05	0.02	−57.26%
Forest	28.56	0.34	98.81%	1.14	0.00	−99.78%
Grassland	680.30	31.96	95.30%	0.49	0.03	−93.99%
Built-up area	10.16	1.09	89.27%	0.43	0.05	−87.69%
sandy land	1803.66	134.81	92.53%	23.77	1.70	−92.87%
Bare soil	336.61	22.73	93.25%	1.45	0.43	−70.50%

4. Discussion

4.1. Contribution of Climatic Drivers

4.1.1. Impacts of Wind Speed on Soil Erosion

The analysis of driving factors showed that climate change is the dominant factor influencing wind erosion changes, which is consistent with previous research findings [44,45]. Overall, climatic variables such as wind speed, precipitation, and temperature influence soil wind erosion in a region [46]. Moreover, weakened atmospheric circulation has caused a significant reduction in near-surface wind speeds over the Tibetan Plateau [47]. Previous research showed that wind speed has a strong impact on dryland soil erosion as it can displace or remove topsoil from the land surface [48]. In addition, the impact of wind speed on wind erosion is the strongest among the climatic factors. A high value of wind speed is

widely distributed on the south bank of the river, indicating that changes in wind speed in this region play a dominant role in wind erosion. Between 1990 and 2020, the average wind speed in the YZRB region was 1.53 m/s, with 79.36% of the area experiencing a decrease in wind speed (Figure 7b). The results of the simple correlation between wind speed and wind erosion also showed a high correlation (Figure 5b). In conclusion, the decrease in wind speed is a crucial factor contributing to the significant reduction in wind erosion. The current regional climate conditions suggest a declining trend in wind speed, which is highly favorable for preventing wind erosion and supports various ecological engineering projects in the YZRB region.

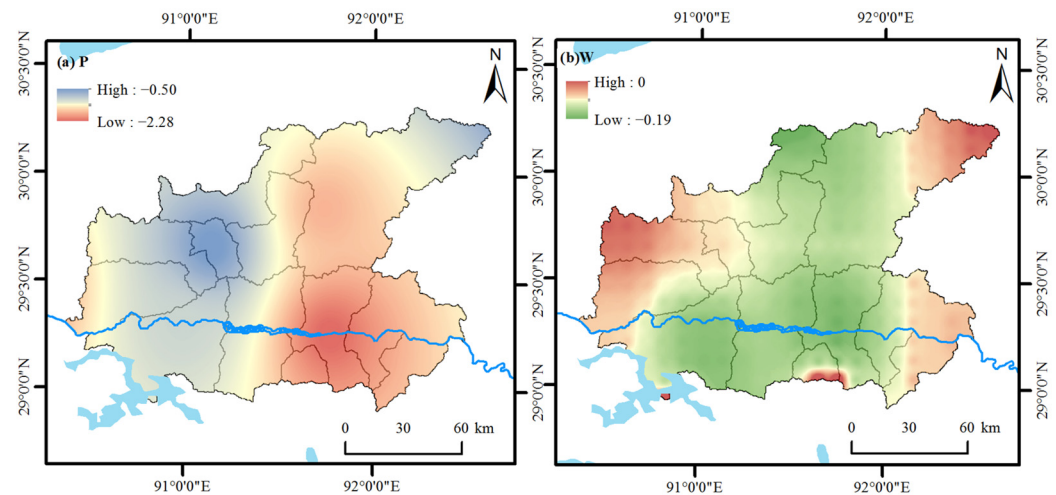


Figure 7. The spatial patterns of the change in slope of precipitation (P) and maximum wind speed (W) in the YZRB area from 1990 to 2020.

4.1.2. Impacts of Precipitation on Soil Wind Erosion

There is a negative relationship between precipitation and wind erosion in most areas [45,49,50]. In contrast, with the decrease in precipitation, wind erosion also decreased in local areas, suggesting that annual precipitation is not the main basic factor determining wind erosion in TP [45], which is consistent with the results of this study. This study has explored a significant decrease in wind erosion with a very low contribution (0.67%) of precipitation to the change, indicating that the impact of precipitation is less significant. The frequency of extreme precipitation events is increasing with global warming [51]. Despite the overall warm and humid trend of TP, some specific regions exhibited a decreasing trend during a certain period. Figure 7a illustrates a slight downward trend in precipitation in the YZRB region, especially in the eastern part. Between 1990 and 2020, there was a slight decrease in precipitation in the YZRB region, with a slope of $-2.28 \sim -0.50 \text{ mm} \cdot \text{a}^{-1}$, which is inconsistent with the results of Zhang [34]. This discrepancy may be attributed to Zhang's selected period of 1979–2018 in the same area, which differs from the time period for this study. There is a temporal heterogeneity in precipitation variations at different time scales [52], providing some insights into the changes in precipitation trends observed in this study.

4.2. Contribution of Non-Climatic Drivers

The trend of SWEM exhibits a strong correlation with precipitation and vegetation coverage on the Tibetan Plateau [45]. Surface vegetation plays a crucial role in determining the intensity of wind erosion, as mentioned by previous research [53]. In recent decades, there has been an improvement in vegetation cover on the Tibetan Plateau [54]. Research has indicated that the recent greening observed on the Tibetan Plateau can be attributed primarily to climate warming, increased humidity, and ecological restoration efforts [33]. The presence of vegetation can greatly enhance aerodynamic roughness and decrease wind speed close to the surface [55,56]. Usually, FVC is an important index that comprehensively

reflects vegetation dynamics and the soil conservation function. And the wind erosion will reduce with the increasing FVC [45]. Our research results show an increasing trend in FVC, with a slight rise on the north bank and a slight decrease away from the water system on the south bank (Figure 8b). The significant increase in FVC may be related to the implementation of ecological engineering.

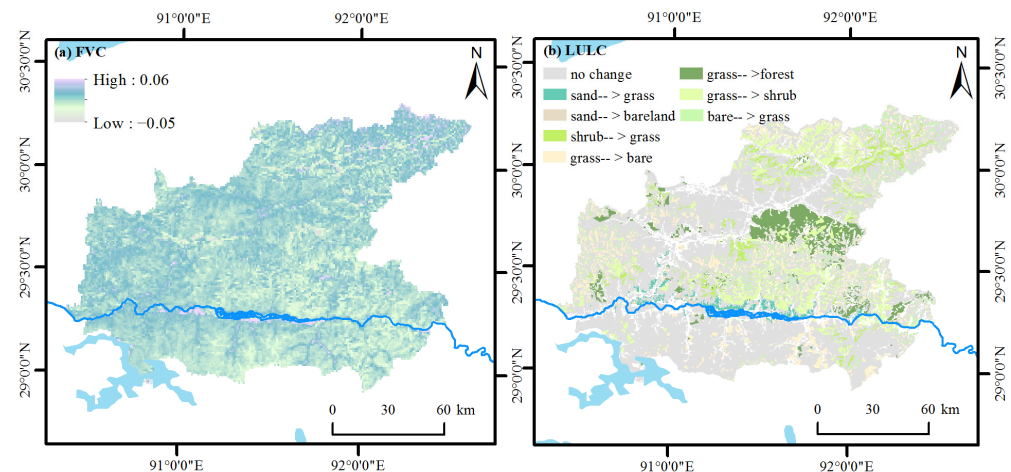


Figure 8. The spatial patterns of LULC (a) and the change in slope of FVC (b) in YZR from 1990 to 2020.

The local government has initiated numerous projects focusing on ecological protection and construction since the 1980s to control desertification and grassland degradation in the Tibetan Plateau [57]. These undertakings involve the plantation of artificial forests, shrubs, and grass to stabilize the sandy land. Afforestation holds significant importance in several aspects, such as carbon sequestration [58,59], control of desertification [60], enhancement of soil [61], regulation of climate [62,63], and preservation of biodiversity [64,65]. Moreover, the previous study [66] reported that afforestation is one of the most effective methods to control desertification in the YZR region. According to statistics, the afforestation area had accumulated to around 175,733.73 ha by 2018 [67]. The implementation of these ecological projects has effectively increased FVC and improved regional vegetation, aligning with the findings of Chen [68]. This indicates that the increase in FVC is primarily driven by human activities.

Furthermore, Pearson correlation analysis between the area of plantation and wind erosion reveals a highly significant negative correlation (-0.638^{**} , $p < 0.01$). This indicates that plantation activities have a significant impact on mitigating wind erosion. It further demonstrates that the implementation of ecological engineering projects has made a substantial and unprecedented contribution to reducing regional wind erosion.

Additionally, the LULC and the trend of FVC had strong consistency in this study. Since 2015, the implementation of a series of measures to combat desertification in the YZR region has resulted in a reduction in sandy land area [28]. As indicated by Figure 9b, the area of forestland and grassland has increased among the LULC. Spatially, 63.25% of bare land is converted into grassland and shrub land, particularly in the northern parts of Chanang County and Nedong County. During this period, many sandy areas also changed significantly, being transformed into grassland and forest land through the implementation of ecological engineering projects. Moreover, there was a significant increase in the shrub land area, with a growth rate of 83.26%. These results indicate the positive role of LULC in reducing soil wind erosion in ecological engineering, which is consistent with similar studies [20,21].

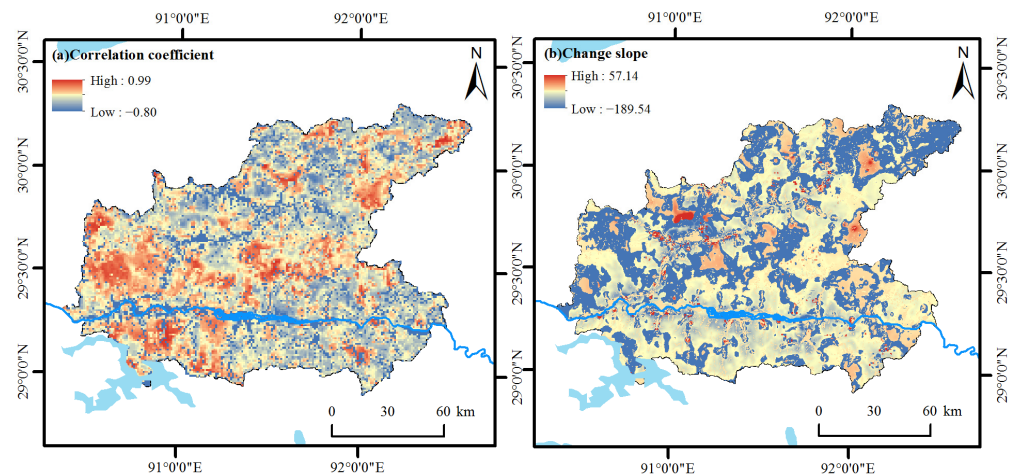


Figure 9. Variations in livestock and relationships with wind erosion in YZRB from 1990 to 2020. (a) the coefficient between the change in livestock and wind erosion; (b) the change in livestock slope.

Apart from afforestation projects, the implementation of the Grazing Forbidden Policy is another significant initiation for ecological engineering management. Previous studies have indicated that grazing can lead to vegetation deterioration and increased wind erosion [69–73]. Our research results indicated an overall decreasing trend in grazing over the past 30 years in this study area. However, there was still spatial heterogeneity in the relationship between grazing and wind erosion. The sloping area neighbouring the valley exhibited severe wind erosion and a positive correlation with grazing (Figure 9a), while the area near the forest showed a negative correlation. This suggests that grazing does not significantly contribute to wind erosion within the floodplain. However, the areas outside the floodplain are crucial for the implementation of the Grazing Forbidden Policy. This study demonstrates that human interventions, such as policy endorsement and associated ecological projects, have effectively restored the plateau vegetation [68].

4.3. Implications

There are still some limitations to this study. Firstly, seasonal differences in wind erosion could not be assessed due to a lack of on-site observation data and the seasonal variation of wind speed thresholds. Secondly, the resolution of experimental data may affect the accurate characterization of the actual distribution of various factors. Hence, future research should consider detailed studies using improved spatial and temporal resolution of input data. In addition, the subjectivity of factor selection for driving factors may not accurately capture all the driving forces as well as controlled intervals of wind erosion. Furthermore, a more in-depth discussion is needed on how to enhance the explanatory power of wind erosion changes through factor interaction to improve the practical reference value of the research. Finally, the driving factors of wind erosion in the YZRB region were identified using partial correlation analysis and complex correlation analysis; however, the coupling effect of climate change and human activities needs to be quantified in further research.

5. Conclusions

In this study, we assessed the spatial and temporal dynamics of soil wind erosion in the YZRB region for the period 1990–2020 using the RWEQ model. Furthermore, we discriminated and quantified the relative effects of climate change and anthropogenic activity on wind erosion. The wind erosion in the YZRB region decreased significantly, with an annual decreasing rate of $-0.912 \text{ t} \cdot \text{hm}^{-2} \cdot \text{a}^{-1}$ and 55.71% of the area showing a significant downward trend. Moreover, the trend of wind erosion is still dominated by a continuous decline in areas with frequent anthropogenic activities. The severe intensity of soil wind erosion is mainly concentrated in the flat and broad river valley. This study

further revealed that sandy land exhibited higher reduction rates in soil wind erosion modulus, with reduction rates of 92.87%. Through analysis of the relationships among wind erosion, climatic factors, and anthropogenic activities, we found that climate change was the dominant factor controlling changes in wind erosion over the YZRB region. In the significantly reduced area, the decreased maximum wind speed influenced the wind erosion outstandingly, indicating the important role of climate change. While human activities accounted for 43.50% of the wind erosion variations in YZRB, they were closely related to the LULC, which is mostly distributed in the implementation area of ecological engineering projects. During the last 30 years, the observed reductions in wind speed and the implementation of ecological restoration programs have generally lessened wind erosion. Ecological restoration programs have a positive contribution to make in decreasing wind erosion and reversing the trend of grassland degradation.

Author Contributions: Conceptualization, D.X. and X.Q.; methodology, X.Q. and D.Z.; software, X.Q. and D.Z.; validation, X.Q., W.Z. and S.L.; formal analysis, X.Q. and Z.Y.; investigation, X.Q. and D.Z.; resources, D.X. and B.Z.; data curation, X.Q. and Z.Y.; writing—original draft preparation, X.Q., D.X., L.L. and D.Z.; writing—review and editing, X.Q. and D.Z.; visualization, X.Q. and D.K.R.; supervision, D.X. and B.Z.; project administration, D.X. and W.D.; funding acquisition, D.X., W.D. and B.Z. All authors have read and agreed to the published version of the manuscript.

Funding: This study was jointly funded by the Key Program of the National Natural Science Foundation of China (grant number 41930651) and the Second Tibetan Plateau Scientific Expedition and Research Program (STEP) (2019QZKK0404).

Data Availability Statement: Not applicable.

Acknowledgments: We would like to thank all the anonymous reviewers who comprehensively contributed to this paper by providing valuable suggestions and comments, as well as the editors for their editing work on the manuscript. The financial support from the Key Program of the National Natural Science Foundation of China (grant number 41930651) and the Second Tibetan Plateau Scientific Expedition and Research Program (2019QZKK0404) are gratefully acknowledged.

Conflicts of Interest: The authors declare no conflict of interest.

References

1. Lal, R. Soil erosion and the global carbon budget. *Environ. Int.* **2003**, *29*, 437–450. [\[CrossRef\]](#)
2. Pimentel, D.; Harvey, C.; Resosudarmo, P.; Sinclair, K.; Kurz, D.; McNair, M.; Crist, S.; Shpritz, L.; Fitton, L.; Saffouri, R. Environmental and Economic Costs of Soil Erosion and Conservation Benefits. *Science* **1995**, *267*, 1117–1123. [\[CrossRef\]](#)
3. Zhou, Z.; Zhang, Z.; Zou, X.; Zhang, K.; Zhang, W. Quantifying wind erosion at landscape scale in a temperate grassland: Nonignorable influence of topography. *Geomorphology* **2020**, *370*, 107401. [\[CrossRef\]](#)
4. Gholami, H.; Mohamadifar, A.; Bui, D.T.; Collins, A.L. Mapping wind erosion hazard with regression-based machine learning algorithms. *Sci. Rep.* **2020**, *10*, 20494. [\[CrossRef\]](#) [\[PubMed\]](#)
5. Zhao, Y.; Wu, J.; He, C.; Ding, G. Linking wind erosion to ecosystem services in drylands: A landscape ecological approach. *Landsc. Ecol.* **2017**, *32*, 2399–2417. [\[CrossRef\]](#)
6. Pi, H.; Sharratt, B.; Lei, J. Wind erosion and dust emissions in central Asia: Spatiotemporal simulations in a typical dust year. *Earth Surf. Process. Landf.* **2019**, *44*, 521–534. [\[CrossRef\]](#)
7. Li, H.; Tatarko, J.; Kucharski, M.; Dong, Z. PM_{2.5} and PM₁₀ emissions from agricultural soils by wind erosion. *Aeolian Res.* **2015**, *19*, 171–182. [\[CrossRef\]](#)
8. Todhunter, P.E.; Cihacek, L.J. Historical reduction of airborne dust in the Red River Valley of the North. *J. Soil Water Conserv.* **1999**, *54*, 543–551. [\[CrossRef\]](#)
9. Sharratt, B.; Tatarko, J.; Abatzoglou, J.; Fox, F.; Huggins, D. Implications of climate change on wind erosion of agricultural lands in the Columbia plateau. *Weather. Clim. Extrem.* **2015**, *10*, 20–31. [\[CrossRef\]](#)
10. Zhao, C.; Zhang, H.; Wang, M.; Jiang, H.; Wang, Y. Impacts of climate change on wind erosion in southern Africa between 1991 and 2015. *Land Degrad. Dev.* **2020**. [\[CrossRef\]](#)
11. He, J.J.; Cai, Q.G.; Cao, W.Q. Wind tunnel study of multiple factors affecting wind erosion from cropland in agro-pastoral area of Inner Mongolia, China. *J. Mt. Sci.* **2013**, *10*, 68–74. [\[CrossRef\]](#)
12. Wei, W.; Chen, L.; Fu, B.; Chen, J. Water erosion response to rainfall and land use in different drought-level years in a loess hilly area of China. *Catena* **2010**, *81*, 24–31. [\[CrossRef\]](#)
13. Snyder, K.A.; Tartowski, S.L. Multi-scale temporal variation in water availability: Implications for vegetation dynamics in arid and semi-arid ecosystems. *J. Arid. Environ.* **2006**, *65*, 219–234. [\[CrossRef\]](#)

14. Wasson, R.J.; Nanninga, P.M. Estimating wind transport of sand on vegetated surfaces. *Earth Surf. Process. Landf.* **1986**, *11*, 505–514. [\[CrossRef\]](#)
15. Li, F.R.; Kang, L.F.; Zhang, H.; Zhao, L.Y.; Shirato, Y.; Taniyama, I. Changes in intensity of wind erosion at different stages of degradation development in grasslands of Inner Mongolia, China. *J. Arid. Environ.* **2005**, *62*, 567–585. [\[CrossRef\]](#)
16. Lancaster, N.; Baas, A. Influence of vegetation cover on sand transport by wind: Field studies at Owens Lake, California. *Earth Surf. Process. Landf.* **2015**, *23*, 69–82. [\[CrossRef\]](#)
17. Yan, Y.; Xu, X.; Xin, X.; Yang, G.; Chen, B. Effect of vegetation coverage on aeolian dust accumulation in a semiarid steppe of northern China. *Catena* **2011**, *87*, 351–356. [\[CrossRef\]](#)
18. Cao, F.; Dan, L.; Ma, Z.; Gao, T. Assessing the regional climate impact on terrestrial ecosystem over East Asia using coupled models with land use and land cover forcing during 1980–2010. *Sci. Rep.* **2020**, *10*, 2572. [\[CrossRef\]](#) [\[PubMed\]](#)
19. Lin, J.; Guan, Q.; Pan, N.; Zhao, R.; Xu, C. Spatiotemporal Variations and Driving Factors of the Potential Wind Erosion Rate in the Hexi Region. *Land Degrad. Dev.* **2020**, *32*, 139–157. [\[CrossRef\]](#)
20. Chi, W.; Zhao, Y.; Kuang, W.; He, H. Impacts of anthropogenic land use/cover changes on soil wind erosion in China. *Sci. Total Environ.* **2019**, *668*, 204–215. [\[CrossRef\]](#)
21. Zhao, Y.; Chi, W.; Kuang, W.; Bao, Y.; Ding, G. Ecological and environmental consequences of ecological projects in the Beijing–Tianjin sand source region. *Ecol. Indic.* **2020**, *112*, 106111. [\[CrossRef\]](#)
22. Yan, F.; Wu, B.; Wang, Y. Estimating spatiotemporal patterns of aboveground biomass using Landsat TM and MODIS images in the Mu Us Sandy Land, China. *Agric. For. Meteorol.* **2015**, *200*, 119–128. [\[CrossRef\]](#)
23. Tian, D. Nonlinear responses of ecosystem carbon fluxes and water-use efficiency to nitrogen addition in Inner Mongolia grassland. *Funct. Ecol.* **2016**, *30*, 490–499. [\[CrossRef\]](#)
24. Huang, K.; Zhang, Y.; Zhu, J.; Liu, Y.; Zu, J.; Zhang, J. The influences of climate change and human activities on vegetation dynamics in the Qinghai-Tibet Plateau. *Remote Sens.* **2016**, *8*, 876. [\[CrossRef\]](#)
25. Wang, Z.; Silva, L.C.; Sun, G.; Luo, P.; Mou, C.; Horwath, W.R. Quantifying the impact of drought on soil-plant interactions: A seasonal analysis of biotic and abiotic controls of carbon and nutrient dynamics in high-altitudinal grasslands. *Plant Soil* **2015**, *389*, 59–71. [\[CrossRef\]](#)
26. Liu, H.; Li, X.; Xiao, J. Variations of Wind Erosion Climatic Erosivity in the Yarlung Zangbo River Basin During 1961–2015. *Sci. Geogr. Sin.* **2019**, *39*, 688–695. [\[CrossRef\]](#)
27. Dong, G.R.; Dong, Y.X.; Li, S.; Jin, J.; Liu, Y.Z. The causes and developmental trend of desertification in the middle reaches of the Yarlung Zangbo River and its two tributaries in Xizang. *Chin. Geogr. Sci.* **1995**, *5*, 355–364. [\[CrossRef\]](#)
28. Zhan, Q.; Zhao, W.; Yang, M.; Xiong, D. A long-term record (1995–2019) of the dynamics of land desertification in the middle reaches of Yarlung Zangbo River basin derived from Landsat data. *Geogr. Sustain.* **2021**, *2*, 12–21. [\[CrossRef\]](#)
29. Immerzeel, W.W.; Lutz, A.F.; Andrade, M.; Bahl, A.; Baillie, J.E.M. Importance and vulnerability of the world’s water towers. *Nature* **2020**, *577*, 364–369. [\[CrossRef\]](#)
30. Pepin, N.; Bradley, R.S.; Diaz, H.F.; Baraer, M.; Caceres, E.B.; Forsythe, N.; Fowler, H.; Greenwood, G.; Hashmi, M.Z.; Liu, X.D. Elevation-dependent warming in mountain regions of the world. *Nat. Clim. Chang.* **2015**, *5*, 424–430. [\[CrossRef\]](#)
31. Yang, K.; Wu, H.; Qin, J.; Lin, C.; Tang, W.; Chen, Y. Recent climate changes over the Tibetan Plateau and their impacts on energy and water cycle: A review. *Glob. Planet. Chang.* **2014**, *112*, 79–91. [\[CrossRef\]](#)
32. Kuang, W.; Liu, J.; Dong, J.; Chi, W.; Zhang, C. The rapid and massive urban and industrial land expansions in China between 1990 and 2010: A CLUD-based analysis of their trajectories, patterns, and drivers. *Landsc. Urban Plan.* **2016**, *145*, 21–33. [\[CrossRef\]](#)
33. Li, Q.; Zhang, C.; Shen, Y.; Jia, W.; Li, J. Quantitative assessment of the relative roles of climate change and human activities in desertification processes on the Qinghai-Tibet Plateau based on net primary productivity. *Catena* **2016**, *147*, 789–796. [\[CrossRef\]](#)
34. Zhang, B.; Xiong, D.; Tang, Y.; Liu, L. Land surface roughness impacted by typical vegetation restoration projects on aeolian sandy lands in the Yarlung Zangbo River valley, southern Tibetan plateau. *Int. Soil Water Conserv. Res.* **2022**, *10*, 109–118. [\[CrossRef\]](#)
35. Li, H.; Shen, W.; Zou, C.; Jiang, J.; Fu, L.; She, G. Spatio-temporal variability of soil moisture and its effect on vegetation in a desertified aeolian riparian ecotone on the Tibetan Plateau, China. *J. Hydrol.* **2013**, *479*, 215–225. [\[CrossRef\]](#)
36. Shen, W.; Li, H.; Sun, M.; Jiang, J. Dynamics of aeolian sandy land in the Yarlung Zangbo River basin of Tibet, China from 1975 to 2008. *Glob. Planet. Chang.* **2012**, *86*, 37–44. [\[CrossRef\]](#)
37. Fryrear, D.W.; Bilbro, J.D.; Saleh, A.; Schomberg, H.; Stout, J.E.; Zobeck, T.M. RWEQ: Improved wind erosion technology. *J. Soil Water Conserv.* **2000**, *55*, 183–189.
38. Jarrah, M.; Mayel, S.; Tatarko, J.; Funk, R.; Kuka, K. A review of wind erosion models: Data requirements, processes, and validity. *Catena* **2019**, *187*, 104388. [\[CrossRef\]](#)
39. Kendall, M.G. Rank Correlation Methods. *Br. J. Psychol.* **1990**, *25*, 86–91. [\[CrossRef\]](#)
40. Mann, H.B. Nonparametric test against trend. *Econometrica* **1945**, *13*, 245–259. [\[CrossRef\]](#)
41. Sen, P.K. Estimates of the Regression Coefficient Based on Kendall’s Tau. *Publ. Am. Stat. Assoc.* **1968**, *63*, 1379–1389. [\[CrossRef\]](#)
42. The Hurst phenomenon and the rescaled range statistic. Stochastic Processes and Their Applications: An Official. *J. Bernoulli Soc. Math. Stat. Probab.* **2016**, *126*, 3790–3807. [\[CrossRef\]](#)
43. Sen, L.I. Classification and development of aeolian sand landform in the Yurlung Zangbo Vally. *J. Desert Res.* **1997**, *17*, 342. [\[CrossRef\]](#)
44. Xie, S.; Qu, J.; Xu, X.; Pang, Y. Interactions between freeze–thaw actions, wind erosion desertification, and permafrost in the Qinghai–Tibet Plateau. *Nat. Hazards* **2017**, *85*, 829–850. [\[CrossRef\]](#)

45. Teng, Y.; Zhan, J.; Liu, W.; Sun, Y.; Agyemang, F.B.; Liang, L.; Li, Z. Spatiotemporal dynamics and drivers of wind erosion on the Qinghai-Tibet Plateau, China. *Ecol. Indic.* **2021**, *123*, 107340. [[CrossRef](#)]
46. Li, J.; Ma, X.; Zhang, C. Predicting the spatiotemporal variation in soil wind erosion across Central Asia in response to climate change in the 21st century. *Sci. Total Environ.* **2019**, *709*, 136060. [[CrossRef](#)] [[PubMed](#)]
47. Duan, A.; Wu, G. Weakening trend in the atmospheric heat source over the Tibetan Plateau during recent decades. Part II: Connection with climate warming. *J. Clim.* **2009**, *22*, 4197–4212. [[CrossRef](#)]
48. Tegen, I.; Lacis, A.A.; Fung, I. The influence on climate forcing of mineral aerosols from disturbed soils. *Nature* **1996**, *380*, 419–422. [[CrossRef](#)]
49. Wu, X.; Fan, J.; Sun, L.; Zhang, H.; Chi, W. Wind erosion and its ecological effects on soil in the northern piedmont of the Yinshan Mountains. *Ecol. Indic.* **2021**, *128*, 107825. [[CrossRef](#)]
50. Jiang, Y.; Gao, Y.; Dong, Z.; Liu, B.; Zhao, L. Simulations of wind erosion along the Qinghai-Tibet Railway in north-central Tibet. *Aeolian Res.* **2018**, *32*, 192–201. [[CrossRef](#)]
51. Davis, C.J.; Hanna, E.G. Seasonal temperature and rainfall extremes 1911–2017 for Northern Australian population centres: Challenges for human activity. *Reg. Environ. Chang.* **2020**, *20*, 128. [[CrossRef](#)]
52. Zhao, X.; Li, Z.; Zhu, Q. Change of precipitation characteristics in the water-wind erosion crisscross region on the Loess Plateau, China, from 1958 to 2015. *Sci. Rep.* **2017**, *7*, 8048. [[CrossRef](#)]
53. Li, J.; Okin, G.S.; Alvarez, L.; Epstein, H. Quantitative effects of vegetation cover on wind erosion and soil nutrient loss in a desert grassland of southern New Mexico, USA. *Biogeochemistry* **2007**, *85*, 317–332. [[CrossRef](#)]
54. Peng, J.; Liu, Z.; Liu, Y.; Wu, J.; Han, Y. Trend analysis of vegetation dynamics in Qinghai–Tibet Plateau using Hurst Exponent. *Ecol. Indic.* **2012**, *14*, 28–39. [[CrossRef](#)]
55. Leenders, J.K.; Boxel, J.H.V.; Sterk, G. The effect of single vegetation elements on wind speed and sediment transport in the Sahelian zone of Burkina Faso. *Earth Surf. Process. Landf.* **2010**, *32*, 1454–1474. [[CrossRef](#)]
56. Liu, J.; Kimura, R.; Miyawaki, M.; Kinugasa, T. Effects of plants with different shapes and coverage on the blown-sand flux and roughness length examined by wind tunnel experiments. *Catena* **2021**, *197*, 104976. [[CrossRef](#)]
57. Wu, Y. *The Study on the Relationship between Ecological Conservation and Rural Households' Income Improvement in Tibet*; Beijing Forestry University: Beijing, China, 2016.
58. Richter, D.D.; Markewitz, D.; Trumbore, S.E.; Wells, C. Rapid accumulation and turnover of soil carbon in a re-establishing forest. *Nature* **1999**, *400*, 56–58. [[CrossRef](#)]
59. Chen, J.M. Carbon neutrality: Toward a sustainable future. *Innovation* **2021**, *2*, 100127. [[CrossRef](#)]
60. Ma, Q.; Fehmi, J.S.; Zhang, D.; Fan, B.; Chen, F. Changes in wind erosion over a 25-year restoration chronosequence on the south edge of the Tengger Desert, China: Implications for preventing desertification. *Environ. Monit. Assess.* **2017**, *189*, 463. [[CrossRef](#)]
61. Tao, W. Progress in sandy desertification research of China. *J. Geogr. Sci.* **2004**, *14*, 387–400. [[CrossRef](#)]
62. Doelman, J.C.; Stehfest, E.; van Vuuren, D.P.; Tabeau, A.; Hof, A.F.; Braakhekke, M.C.; Gernaat, D.; van den Berg, M.; van Zeist, W.-J.; Daioglou, V.; et al. Afforestation for climate change mitigation: Potentials, risks and trade-offs. *Glob. Chang. Biol.* **2020**, *26*, 1576–1591. [[CrossRef](#)] [[PubMed](#)]
63. Yang, M.; Zhao, W.; Zhan, Q.; Xiong, D. Spatiotemporal Patterns of Land Surface Temperature change in the Tibetan Plateau Based on MODIS/Terra Daily Product from 2000 to 2018. *IEEE J. Sel. Top. Appl. Earth Obs. Remote Sens.* **2021**, *14*, 6501–6514. [[CrossRef](#)]
64. Wardle, D.A.; Bonner, K.I.; Barker, G.M.; Yeates, G.W.; Nicholson, K.S.; Bardgett, R.D.; Watson, R.N.; Ghani, A. Plant removals in perennial grassland: Vegetation dynamics, decomposers, soil biodiversity, and ecosystem properties. *Ecol. Monogr.* **1999**, *69*, 535–568. [[CrossRef](#)]
65. Li, X.R.; Zhang, J.G.; Liu, L.C.; Chen, H.S.; Shi, Q.H. Plant Diversity and Succession of Artificial Vegetation Types and Environment in an Arid Desert Region of China. In *Conserving Biodiversity in Arid Regions*; Springer: New York, NY, USA, 2000; pp. 179–188. [[CrossRef](#)]
66. Fu, H.; Zhao, W.; Zhan, Q.; Yang, M.; Xiong, D.; Yu, D. Temporal Information Extraction for Afforestation in the Middle Section of the Yarlung Zangbo River Using Time-Series Landsat Images Based on Google Earth Engine. *Remote Sens.* **2021**, *13*, 4785. [[CrossRef](#)]
67. Zhao, D.; Xiong, D.; Zhang, B.; He, K.; Wu, H.; Zhang, W.; Lu, X. Long-term response of runoff and sediment load to spatiotemporally varied rainfall in the Lhasa River basin, Tibetan Plateau. *J. Hydrol.* **2023**, *618*, 129154. [[CrossRef](#)]
68. Chen, B.; Zhang, X.; Tao, J.; Wu, J.; Wang, J.; Shi, P.; Zhang, Y.; Yu, C. The impact of climate change and anthropogenic activities on alpine grassland over the Qinghai-Tibet Plateau. *Agric. For. Meteorol.* **2014**, *189*, 11–18. [[CrossRef](#)]
69. Du, H.; Zuo, X.; Li, S.; Wang, T.; Xue, X. Wind erosion changes induced by different grazing intensities in the desert steppe, Northern China. *Agric. Ecosyst. Environ.* **2019**, *274*, 1–13. [[CrossRef](#)]
70. Sato, C.F.; Strong, C.L.; Holliday, P.; Florance, D.; Pierson, J.; Lindenmayer, D.B. Environmental and grazing management drivers of soil condition. *Agric. Ecosyst. Environ. Int. J. Sci. Res. Relatsh. Agric. Food Prod. Biosph.* **2019**, *276*, 1–7. [[CrossRef](#)]
71. Yu, H.; Li, Y.; Oshunsanya, S.O.; Are, K.S.; Geng, Y.; Saggat, S.; Liu, W. Re-introduction of light grazing reduces soil erosion and soil respiration in a converted grassland on the Loess Plateau, China. *Agric. Ecosyst. Environ.* **2019**, *280*, 43–52. [[CrossRef](#)]

-
72. Zhang, H.; Fan, J.; Cao, W.; Harris, W.; Li, Y.; Chi, W.; Wang, S. Response of wind erosion dynamics to climate change and human activity in Inner Mongolia, China during 1990 to 2015. *Sci. Total Environ.* **2018**, *639*, 1038–1050. [[CrossRef](#)]
 73. Xu, D.; Li, D. Variation of wind erosion and its response to ecological programs in northern China in the period 1981–2015. *Land Use Policy* **2020**, *99*, 104871. [[CrossRef](#)]

Disclaimer/Publisher’s Note: The statements, opinions and data contained in all publications are solely those of the individual author(s) and contributor(s) and not of MDPI and/or the editor(s). MDPI and/or the editor(s) disclaim responsibility for any injury to people or property resulting from any ideas, methods, instructions or products referred to in the content.